



# Strong-axis and weak-axis buckling of Buckling Restrained Braces under bidirectional loading

*J. Cui, C.-L. Lee & G. MacRae*

Department of Civil and Natural Resources Engineering, University of Canterbury, Christchurch

## ABSTRACT

Buckling Restrained Braces (BRBs) are required to act robustly during an earthquake. Some previous experiments showed that BRBs would buckle about the weak-axis, as well as about the strong-axis. It is believed that bidirectional loading will reduce the stability and strength of the BRB and the aim of this study is to investigate numerically these buckling phenomena under bidirectional loading. Numerical simulations show that a BRB would buckle about its weak axis and strong axis with different wavelengths successively and the wavelengths are not uniform throughout the length of steel core because of the friction force between steel core and concrete. Since out-of-plane loading will reduce the capacity of the BRB, the out-of-plane effect should be considered in the wavelength equation.

*Keywords: Buckling Restrained Braces (BRBs), bidirectional loading, strong-axis and weak-axis buckling, local buckling, wavelength*

## 1 INTRODUCTION

Buckling Restrained Braces (BRBs) and BRB frames (BRBFs) have been widely used in Christchurch rebuild among a variety of new dissipation and base isolation technologies (MacRae & Clifton 2015). For conventional brace, it will buckle before yield. Meanwhile, for BRB, it consists of the steel core, concrete and steel casing. The steel core is used to resist axial load, while the concrete and the steel casing, called restrainer, are used to prevent buckling. Thus, the steel core will experience multi-wave buckling with increasing axial load (see Figure 1).

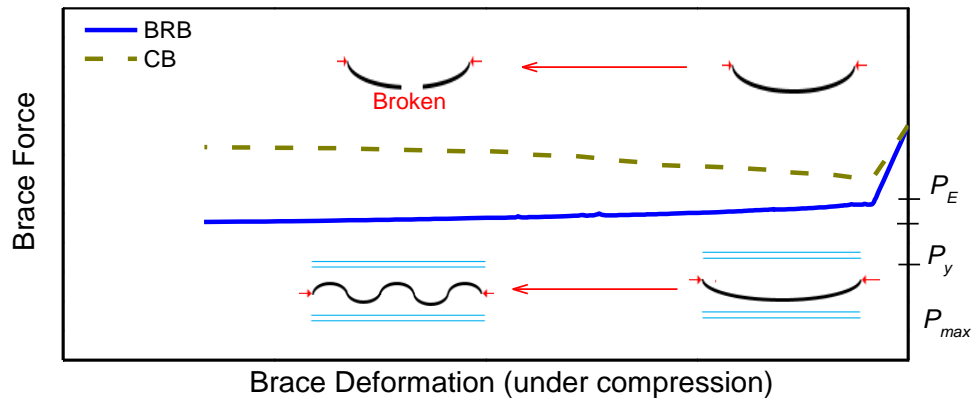


Figure 1: Comparison between BRBF and CBF (CB: Conventional Brace)

The stiffening requirement of the restrainer to prevent the steel core buckling is proposed based on both restrainer stiffness and strength (Inoue et al. 2001). When the stiffness of the restrainer is not enough, global buckling will happen (see type 1, Table 1); when the restrainer is short of strength, local bulging will happen (see type 2, Table 1). Since the local bulging failure has been reported more than global buckling failure in the experiments (Wei & Tsai 2008, Zhao et al. 2014, Lin et al. 2016), it is significant to study the mechanism of local buckling.

Table 1: Two common BRB failure types

Type	Restrainer stiffness	Restrainer strength	Failure type
1	Not Enough	Enough	
2	Enough	Not Enough	

As shown in the experiments by Xu & Pantelides (2017), both strong-axis buckling and weak-axis buckling failures could occur once the confinement at one side is inefficient. They used the angle  $\alpha$  in a strut-and-tie model (see Figure 2) to compute the amount of resistance against the buckling dictates the axis where the buckling occurs about.

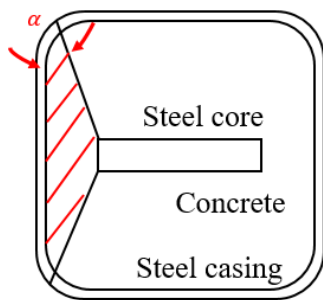


Figure 2: Strut-and-tie models (Xu & Pantelides 2017)

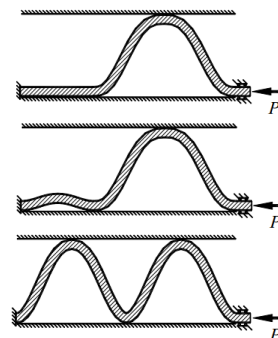


Figure 3: Process of new wave generation (Wu et al. 2012)

One of the critical parameters of local buckling is its wavelength. It is important to know how it can be determined from the geometrical configuration and material properties of the BRB. Zhao et al. (2011) found

in their experiments that the wavelengths are not uniform along the steel core because of the friction between the steel core and the concrete, and the wavelengths at both ends are smaller than that at the middle. An adjustment factor was introduced by them but not well-explained.

Earthquakes could come in any direction with respect to the plane of BRBFs. Therefore, the BRB inside a BRBF could experience not only in-plane (INP) seismic loading but also out-of-plane (OOP) seismic loading. Without considering the OOP loading, the capacity of BRB and BRBF would be overestimated (Cui et al. 2018). Some experimental tests of BRBFs under combined INP and OOP loading have currently been conducted in the University of Canterbury since late 2018 to study the OOP effects.

This study seeks to address the above-mentioned issues through numerical analysis of a BRB specimen being tested in the University of Canterbury. It seeks to answer the following questions:

- 1) What are the impacts of the friction force between the steel core and restrainer?
- 2) What are the effects of OOP displacements on a BRB member under compression?

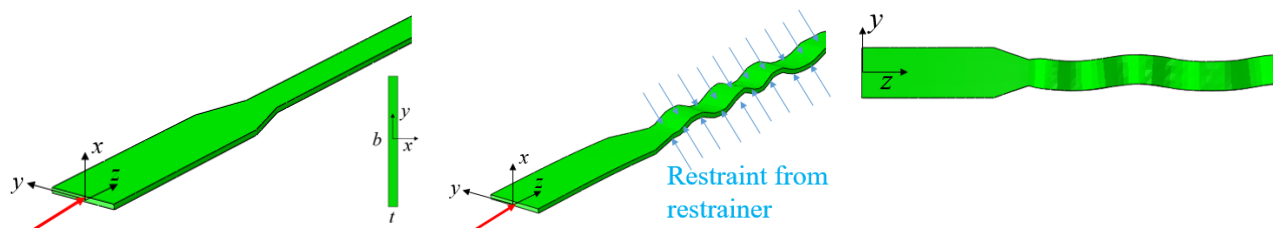
## 2 STRONG-AXIS AND WEAK-AXIS BUCKLING

Wu et al. (2012) explained the process of new wave generation (see Figure 3) and derived the axial loads corresponding to different states (see Equation (1)), where  $P_{n+1}$  is the axial force at the  $n + 1$  waves.  $P_{Es}$  and  $P_{Ew}$  are the critical Euler force when flexural buckling of the steel core about the strong axis and weak axis (see Equation (2)), respectively, assuming the fixed-fixed end condition. And  $b$  and  $t$  are the width and thickness of the steel core.

$$P_{n+1} = (2n + 1)^2 P_E \quad (1)$$

$$P_{Es} = \frac{4\pi^2 E I_s}{L^2} = \frac{\pi^2 E t b^3}{3L^2}, P_{Ew} = \frac{4\pi^2 E I_w}{L^2} = \frac{\pi^2 E b t^3}{3L^2} \quad (2)$$

Since the moment of inertia about the strong axis is greater than that about the weak axis ( $I_s > I_w$ ), a conventional brace will usually buckle about the weak axis. However, for BRB, where core's buckling about the weak axis is restrained by the restrainer (see (b), Figure 4), the steel core will start to buckle about the strong axis with increasing loading (see (c), Figure 4).



(a) Initial state

(b) Buckling about the weak axis

(c) Buckling about the strong axis

Figure 4: Friction force distribution

Takeuchi et al. (2010) approximated the buckling wavelength by applying Euler formula using the BRB yield strength  $P_y$  and the tangent modulus of the steel core  $E_t$ . Based on this approximation, Wu et al. (2014), derived the wavelength equation about both weak-axis  $L_{wm}$  and strong-axis  $L_{sm}$  (see Equation (4), (5)). The equivalent flexural stiffness  $(EI_w)_{eff}$  of the weak axis is assumed equal to 2% of the elastic flexural stiffness  $EI_w$ , while the equivalent flexural stiffness  $(EI_s)_{eff}$  of the strong axis is assumed equal 6% of the elastic flexural stiffness  $EI_s$  using double modulus theory.

$$L_{wm} = \sqrt{\frac{4\pi^2(EI_w)_{eff}}{P_y}} = \sqrt{\frac{4\pi^2 \times 0.06EI_w}{f_ybt}} \quad (3)$$

$$L_{sm} = \sqrt{\frac{4\pi^2(EI_s)_{eff}}{P_y}} = \sqrt{\frac{4\pi^2 \times 0.02EI_s}{f_ybt}} \quad (4)$$

The above equations did not consider the friction between the steel core and the concrete, as well as the OOP loading effect. Since the BRB is locked by a shear key in the middle (see Figure 5), Zhao et al. (2011) deduced that the friction would be progressively transferred from the two ends to the middle and as a result, the two ends would sustain larger axial forces compared with the middle ( $P_M > P_E$ ) (see Figure 6). This non-uniform distribution of the axial force in the steel core leads to different wavelengths. The effects will be investigated further in this study.

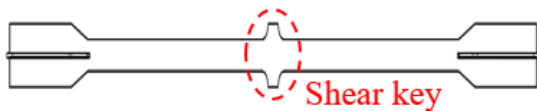


Figure 5: The shear key in a BRB

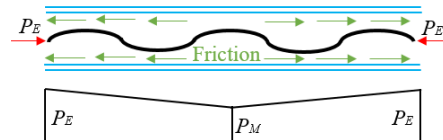


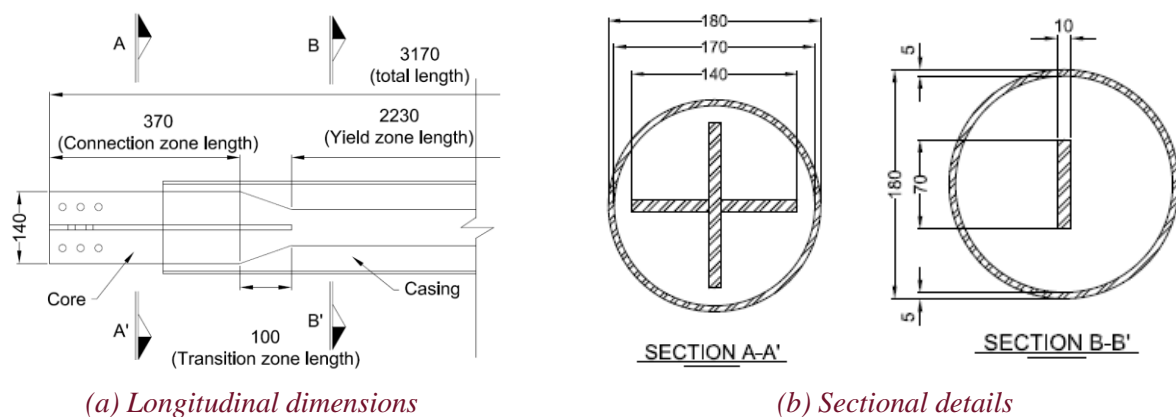
Figure 6: Friction force distribution

### 3 FINITE ELEMENT ANALYSIS OF BRB BUCKLING

#### 3.1 Model introduction

To investigate the effect of the friction and OOP loading on the effective length of BRB, numerical analyses were carried out. A BRB specimen was modelled in Abaqus (Version 6.14) and validated with experimental data.

The steel core is 3170 mm long. Its width and thickness are 70 mm and 10 mm, respectively, in the yielding zone. The casing is 2730 mm long with a circular cross-section, where the outer diameter is 180 mm and thickness is 5 mm (Figure 7).



(a) Longitudinal dimensions

(b) Sectional details

Figure 7: BRB Dimensions and numerical model

The material of the steel core was LY225 steel, a type of low-yield stress steel with the yield strength of 225 MPa. The material property values used in the numerical model were calibrated against the experimental data obtained by Shi et al. (2018). The steel core is modelled using 3D quadratic modified elements (C3D10M). The strength of the concrete restrainer was 40 MPa. The material for the circular casing was Q235B. Both the concrete restrainer and the outer casing were modelled using 3D linear elements (C3D8R)

elements (see Figure 10). Hard contact was used to define the transverse interaction between the steel core and the concrete restrainer. The concrete restrainer is tied to the outer casing.

The BRB specimen was bolted to the gusset plates at both ends, so, it was modelled with a fixed-fixed end condition. A displacement-controlled load was applied to the model. The INP loading  $D_{INP}$  was in the longitudinal direction, i.e. z-direction, while the OOP loading  $D_{OOP}$  was in the x-direction, which is parallel to the strong axis (Figure 8) of the steel core.

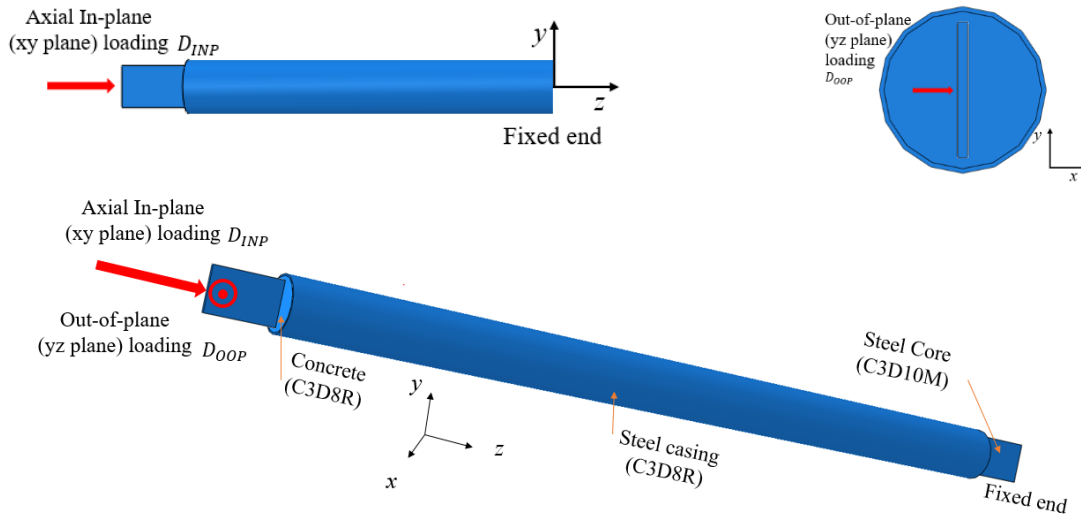


Figure 8: BRB loading conditions and boundary conditions

### 3.2 Model validation

A comparison of the last force-displacement hysteresis loop between the experimental and numerical results is shown in Figure 9 (maximum amplitude of 50 mm, which is equivalent to a storey drift ratio of 2.5%). On the whole, a discrepancy at the bottom left corner is likely caused by the sudden crush between the steel core and concrete in the longitudinal direction due to the careless workmanship for BRB specimen. The remaining part of the curves shows a good agreement between the numerical and the experimental results. In particular, the results show the compressive strength larger than the tensile strength, proving that the friction phenomenon has been well captured in the numerical model. In terms of local behaviour, since the unbonding material was not wrapped properly in the transition zone, only local buckling about the weak axis was found where the effective length is about 95mm (see Figure 10) and the numerical result is close to this number. Thus, the numerical model is now considered validated.

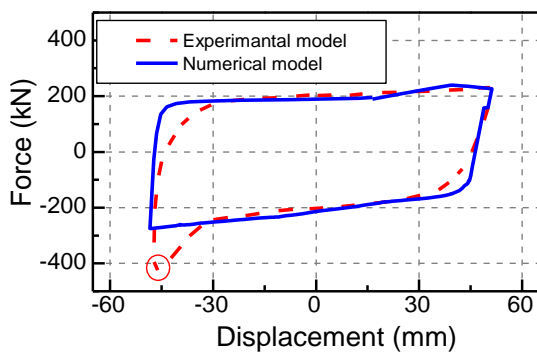


Figure 9: Loading protocol and model calibration (last hysteresis loop)



Figure 10: Effective length measurement for BRB specimen

### 3.3 Loading cases

Five monotonic loading combinations were applied to the BRB model (case 1 - case 5). No OOP loading is considered in case 1. In cases 2 to 5, the ratio of OOP to INP loading increases from 0.5 to 2.0. The displacement-controlled loading will be applied incrementally and proportionally in both INP and OOP directions (see Figure 11).

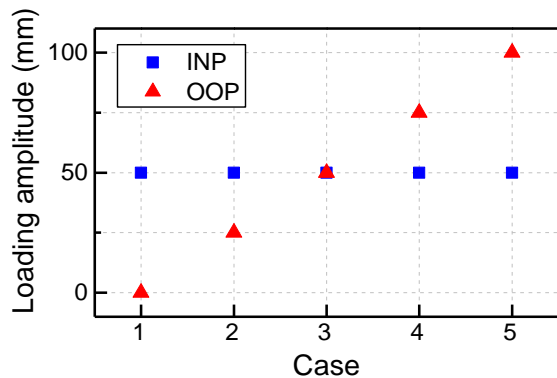


Figure 11: Loading cases

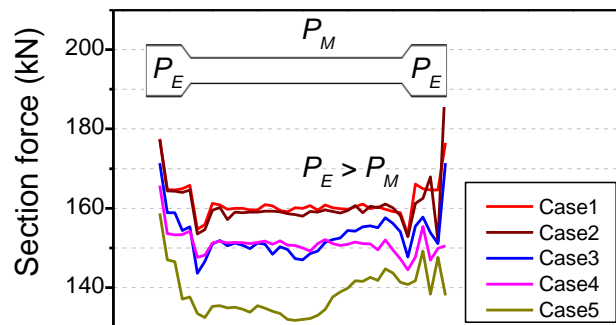
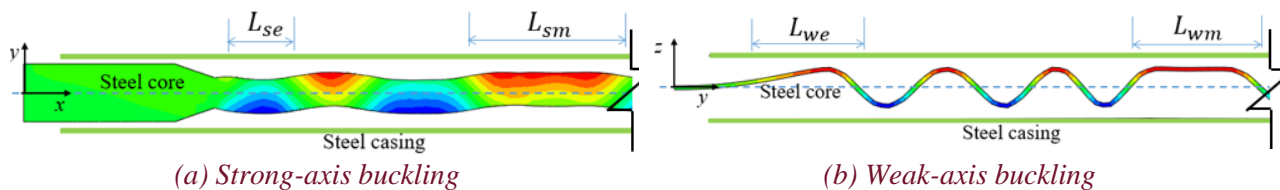


Figure 12: Axial force distribution

## 4 RESULTS

The axial force distribution is shown in Figure 12, it can be seen that the axial force at either end is greater than that in the middle as a result of the presence of friction.

Consider a steel core of rectangular cross-section, Figure 13 shows two examples of its buckling failures about its strong and weak axes. To show the deformed shape of the steel core more directly, a deformation scale factor is used and the concrete is hidden. The local buckling wavelengths about the strong axis at the middle part and the ends are labelled with  $L_{sm}$  and  $L_{se}$ , respectively. They are similarly labelled as  $L_{wm}$  and  $L_{we}$ , for the weak axis.



(a) Strong-axis buckling

(b) Weak-axis buckling

Figure 13: Strong and weak axis buckling

Since the strength is related to the buckling shape of the steel core, its local buckling wavelength will be investigated herein. Figure 14 plots the effective lengths of the steel core under the five loading cases. For the weak-axis buckling, it can be found that:

- 1) A comparison between the effective length in the middle of the core (symbol: black square) and calculated by equation (3) (symbol: blue triangle), current method is conservative because of the small value was used for the tangent modulus, thus a higher tangent modulus is recommended to be used in the calculation;
- 2) By comparing the effective lengths in each case, the effective length at the middle of the steel core is about twice as that at either end ( $L_{wm}/L_{we} \approx 2.0$ );
- 3) From case 1 to case 5, it can be seen that the effective lengths are not affected by the OOP loading increasing.

For the strong-axis buckling, it can be concluded that:

- 1) A comparison between the effective length in the middle of the core (symbol: black square) and calculated by equation (4) (symbol: blue triangle), the current method is applicable when there is axial loading only (case 1);
- 2) By comparing the effective lengths in each case, the effective length at the middle of the steel core is about twice as that at either end ( $L_{sm}/L_{se} \approx 2.0$ );
- 3) From case 1 to case 5, it can be seen that the effective lengths decrease with increasing OOP loading.

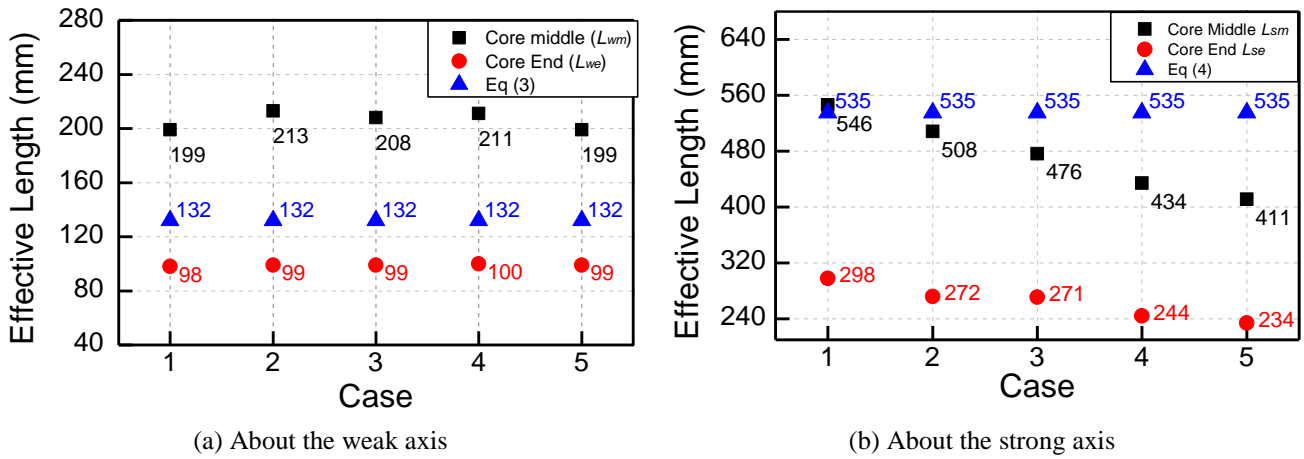


Figure 14: Effective length under different OOP/INP ratios

## 5 DISCUSSIONS

As discussed in previous sections, the wavelengths are different between the end and the middle of the steel core due to the friction. From the numerical results, for both buckling types, the wavelength at the middle is about twice as that at either end, written as:

$$L_{we} = L_{wm}/2 \quad (5)$$

$$L_{se} = L_{sm}/2 \quad (6)$$

To get the effective length in the middle for the weak-axis buckling ( $L_{wm}$ ) and strong axis buckling ( $L_{sm}$ ), Equation (3) still applies to the weak-axis buckling under bidirectional loading since the wavelength is not affected by the OOP loading. A higher tangent modulus is recommended to be used in the calculation, this is because a low-yield point steel is used in this study where the strain hardening factor is greater than other steel types.

The OOP loading will have a big impact on the effective length of the strong-axis buckling. The current method is only applicable to the case where there is no OOP loading. Since no strong axis buckling was found in the authors' current experiment due to the defective BRBs, this phenomenon remains to be further investigated.

## 6 CONCLUSIONS

The main conclusions are:

- 1) Due to the friction between the steel core and the concrete, the wavelength at the middle is about twice as that at the two ends for both strong-axis buckling and weak-axis buckling.
- 2) The OOP loading has little effect on the buckling shape of the weak axis. However, the wavelength of steel core about the strong axis reduces under increasing OOP loading. Current methods need to be improved.

## 7 ACKNOWLEDGEMENT

The authors appreciate the MBIE Natural Hazards Platform (Research Objective 4, New Buildings) for the financial support provided for this study. The authors also acknowledge the funding from HERA and CNRE department of the University of Canterbury for the experimental study.

## REFERENCES

- Cui, J., Lee, C.-L., & MacRae, G. A. 2018. Finite Element Modelling of Buckling Restrained Braces under Combined In-Plane and Out-of-Plane Loading. *Paper presented at The 9th International Conference on Behaviour of Steel Structures in Seismic Areas*, Christchurch, New Zealand.
- Lin, P. C., Tsai, K. C., Chang, C. A., Hsiao, Y. Y., & Wu, A. C. 2016. Seismic design and testing of buckling-restrained braces with a thin profile. *Earthquake Engineering & Structural Dynamics*, 45(3), 339-358.
- Inoue, Kazuo, Shinichi Sawaizumi, and Yasuo Higashibata. "Stiffening requirements for unbonded braces encased in concrete panels." *Journal of structural engineering* 127.6 (2001): 712-719.
- MacRae, G. A., & Clifton, G. C. 2015. Research On Seismic Performance Of Steel Structures. *Paper presented at the Steel Innovations 2015 Conference*, Steel Construction New Zealand, Aotea Centre, Auckland, Christchurch.
- Shi, G., Gao, Y., Wang, X., & Zhang, Y. 2018. Mechanical properties and constitutive models of low yield point steels. *Construction and Building Materials*, 175, 570-587.
- Takeuchi, T., Hajjar, J., Matsui, R., Nishimoto, K., & Aiken, I. 2010. Local buckling restraint condition for core plates in buckling restrained braces. *Journal of constructional steel research*, 66(2), 139-149.
- Wei, C.-Y., & Tsai, K.-C. 2008. Local Buckling of Buckling Restrained Braces. *Paper presented at the The 14th World Conference on Earthquake Engineering*, Beijing, China
- Wu, A. C., Lin, P. C., & Tsai, K. C. 2014. High-mode buckling responses of buckling-restrained brace core plates. *Earthquake Engineering & Structural Dynamics*, 43(3), 375-393.
- Wu, J., Liang, R. J., Wang, C. L., & Shi, J. H. 2012. Research on the multi-wave buckling process of the core component of the buckling-restrained brace. *Engineering Mechanics*, 29(8), 136-142.
- Xu, W., & Pantelides, C. P. 2017. Strong-axis and weak-axis buckling and local bulging of buckling-restrained braces with prismatic core plates. *Engineering Structures*, 153, 279-289.
- Zhao, J., Wu, B., & Ou, J. 2011. Flexural demand on pin-connected buckling-restrained braces and design recommendations. *Journal of Structural Engineering*, 138(11), 1398-1415.
- Zhao, J., Wu, B., Li, W., & Ou, J. 2014. Local buckling behaviour of steel angle core members in buckling-restrained braces: Cyclic tests, theoretical analysis, and design recommendations. *Engineering Structures*, 66, 129-145.